Assembly, Growth, and Catalytic Activity of Gold Nanoparticles in Hollow Carbon Nanofibers

Alessandro La Torre,[†] Maria del Carmen Giménez-López,[†] Michael W. Fay,[‡] Graham A. Rance,[†] William A. Solomonsz,[†] Thomas W. Chamberlain,[†] Paul D. Brown,[§] and Andrei N. Khlobystov[†,*]

[†]School of Chemistry, [‡]Nottingham Nanoscience and Nanotechnology Centre, and [§]Division of Materials, Mechanics and Structures, Department of Mechanical, Materials and Manufacturing Engineering, Faculty of Engineering, University of Nottingham, University Park, Nottingham NG7 2RD, United Kingdom

ABSTRACT Graphitized carbon nanofibers (GNFs) act as efficient templates for the growth of gold nanoparticles (AuNPs) adsorbed on the interior (and exterior) of the tubular nanostructures. Encapsulated AuNPs are stabilized by interactions with the step-edges of the individual graphitic nanocones, of which GNFs are composed, and their size is limited to approximately 6 nm, while AuNPs adsorbed on the atomically flat graphitic surfaces of the GNF exterior continue their growth to 13 nm and beyond under the same heat treatment conditions. The corrugated structure of the GNF interior imposes a significant barrier for the migration of AuNPs, so that their growth mechanism is restricted to Ostwald ripening. Conversely, nanoparticles adsorbed on smooth GNF exterior surfaces are more likely to migrate and coalesce into larger nanoparticles, as revealed by *in situ* transmission electron microscopy imaging. The presence of alkyl thiol surfactant within the GNF channels changes the dynamics of the AuNP transformations, as surfactant molecules adsorbed on the surface of the AuNPs diminished the stabilization effect of the step-edges, thus allowing nanoparticles to grow until their diameters reach the internal diameter of the host nanofiber. Nanoparticles thermally evolved within the GNF channel exhibit alignment, perpendicular to the GNF axis due to interactions with the step-edges and parallel to the axis because of graphitic facets of the nanocones. Despite their small size, AuNPs in GNF possess high stability and remain unchanged at temperatures up to 300 °C in ambient atmosphere. Nanoparticles immobilized at the step-edges within GNF are shown to act as effective catalysts promoting the transformation of dimethylphenylsilane to bis(dimethylphenyl)disiloxane with a greater than 10-fold enhancement of selectivity as compared to free-standing or surface-adsorbed nanoparticles.

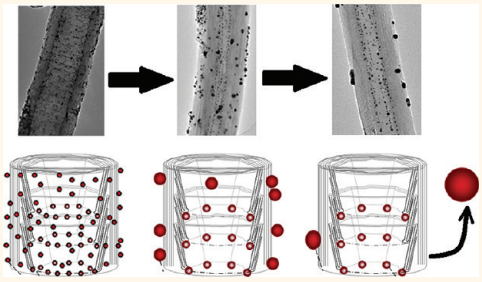

KEYWORDS: carbon nanofibers · gold nanoparticles · encapsulation · nanoparticle growth · nanoparticle assembly · catalysis

Over the past decade, hollow cylindrical nanostructures filled with functional nanoparticles (NPs) have attracted a great deal of attention for their potential applications in different areas of nanotechnology and biomedical sciences.[1−15] Numerous approaches have been proposed for the insertion of nanoparticles into host nanostructures;[16−22] however, gaining control over the size and the position of encapsulated NPs, which are important for catalysis or electronic applications, has not been achieved. To date, only three examples of the encapsulation of preformed, free-standing metal NPs have been reported,[23−25] showing that the size of the inserted NP can be significantly affected by the conditions of their encapsulation into the host structure. Since metal nanoparticles exhibit size-dependent physical and chemical properties, control of size during encapsulation is critical. As carbon nanotubes (CNTs) and graphitized carbon nanofibers (GNFs) are chemically inert, passive containers, they represent the most suitable host material for novel composites where the properties of the guest can either be retained or enhanced depending on synergistic interactions with the host. However, as the NPs in these fascinating hybrid materials are thermodynamically metastable, applications are currently restricted to room temperature to avoid any undesirable NP transformations. There is, therefore, a clear need for the development of new strategies which will broaden the operating temperature range of these materials, while controlling and retaining the NP size and shape if the full scope of the potential applications for these systems is to be realized. Our study aims at understanding the thermally driven growth process of metal NPs adsorbed outside and inside hollow GNFs, revealing different mechanisms for the thermal evolution of NPs. We demonstrate that the growth process and the nanoscale organization of AuNPs depend on and can be controlled by the nature and strength of the interactions between the guest NPs and the host nanocontainers.

* Address correspondence to andrei.khlobystov@nottingham.ac.uk.

Received for review July 28, 2011 and accepted February 22, 2012.

Published online February 22, 2012
10.1021/nn300400z

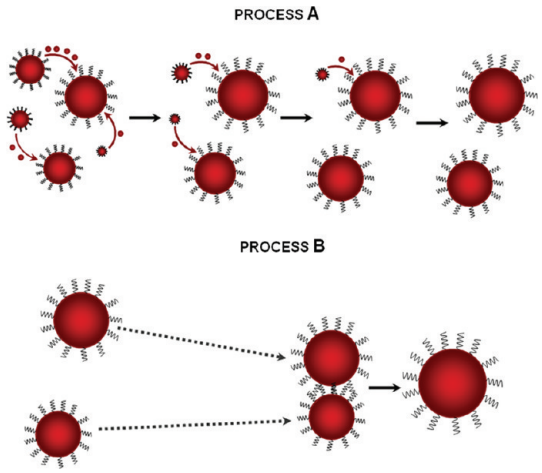

Figure 1. Schematic representation of the two processes responsible for the growth of NPs: (A) Ostwald ripening, where atoms or small clusters of atoms diffuse from smaller to larger NPs, and (B) nanoparticle migration followed by coalescence. In both cases, the overall number of nanoparticles decreases as their average diameter increases.

RESULTS AND DISCUSSION

The growth of NPs adsorbed onto multiwalled carbon nanotubes and other surfaces[26−28] or embedded in polymers[29] has been extensively investigated. Two possible mechanisms have been identified to be responsible for NP growth: (A) Ostwald ripening and (B) particle migration followed by coalescence[30] (Figure 1). Transmission electron microscopy (TEM) is the only technique that is able to visualize directly metal NPs embedded in carbon or organic matrices and to observe their transformations in real space at real time at the near-atomic level. However, so far, the use of TEM is mainly restricted to *ex situ* measurements[31] that limit the level of information obtainable about the actual growth mechanism. *In situ* TEM monitoring of physicochemical processes, however, must be applied with caution, as the energy of the incident electrons of the electron beam (e-beam) may affect the kinetics or mechanism of the process under observation. Hence, real time monitoring of NP growth in carbon nanostructures at the nanoscale, which is crucial for understanding the fundamental mechanism of the process, still remains a challenge.

Small dodecanethiol-stabilized gold NPs[32] (AuNPs) with a core diameter of 2.3 ± 0.4 nm (Supporting Information, Figure S1) were selected for studying the process of NP growth with GNFs. Open, dry GNFs were added to a suspension of AuNPs in a mixture of *n*-pentane and CO_2 in supercritical conditions (pressure 4000 psi, temperature 40 °C) to obtain the AuNP−GNF composite. Supercritical CO_2 ($scCO_2$), possessing very low viscosity and no surface tension, is able to penetrate the entire volume of the GNFs and to deliver AuNPs into their channels as well as to deposit AuNPs on the surface of the GNFs. In the resultant composite material, the nanoparticles are randomly distributed on both surfaces (interior and exterior) of the hollow nanofibers (Figure 2). Detailed analysis of TEM images of the resultant material indicates that the size and shape distribution of the adsorbed AuNPs remain virtually unchanged as compared to the initial, free-standing nanoparticles.

Unlike carbon nanotubes, which consist of concentric tubes of graphene, the structures of the inner and outer GNF's surfaces are fundamentally different to each other. High-resolution TEM (HRTEM) imaging of the internal structure of GNFs produced by chemical vapor deposition (CVD) reveals a structure that can be described as a set of stacked cones of graphene (Figure 3). HRTEM images of the GNF side walls show planes of graphene oriented at an angle of approximately 30° relative to the axis of the main GNF cylinder and faint lines perpendicular to the GNF axis corresponding to the edges of the individual cones that are spaced by 8−15 nm from each other. This succession of stacked cones creates a series of steps along the interior surface of the nanofiber, which can serve as "anchoring points" for molecules and nanoparticles inside the internal channel. In contrast, the outer surface of GNFs consists of a continuous, atomically flat cylindrical layer of graphene.

Thermal energy activates the growth of nanoparticles in the AuNP−GNF composite. AuNP−GNF samples heated in vacuum (*i.e.*, in an evacuated sealed glass ampule using a tube furnace or inside the TEM column using a heated stage TEM holder with the e-beam turned off) at 300 °C for 2 h exhibit a binary mixture of nanoparticles (Figure 2d−f). The initially monodispersed 2.3 nm AuNPs (Figure 2a) are transformed into two distinct groups: 6.4 ± 0.4 nm AuNPs and 13.4 ± 0.6 nm AuNPs. Furthermore, the subset of larger nanoparticles appears to be positioned on the surface of the GNFs, while the subset of smaller ones appears to be located inside the GNFs. However, as TEM images are 2D projections of 3D nanostructures, assignment of the exact location of the individual AuNPs is not entirely unambiguous at this stage.

High-angle annular dark-field (HAADF) scanning transmission electron microscopy (STEM) imaging of a AuNP−GNF composite sample, heat treated at 300 °C in vacuum, at different tilt angles clearly shows that only the 6 nm AuNPs are located in the internal cavity of the GNF (to a level of 500 NPs·μm^{-1}), forming linear arrangements along the nanofiber axis. In contrast, AuNPs with diameters ≥13 nm are randomly distributed on the outer surface of the GNF (Figure 4).

To ensure that the e-beam of the TEM does not cause any changes in the structure of the specimen, the energy of the e-beam was lowered to 100 keV, the flux was kept as low as possible (*ca.* 5pA/cm^2), and the exposure time of the specimen to the e-beam was kept to a minimum (only during the image capture). Under

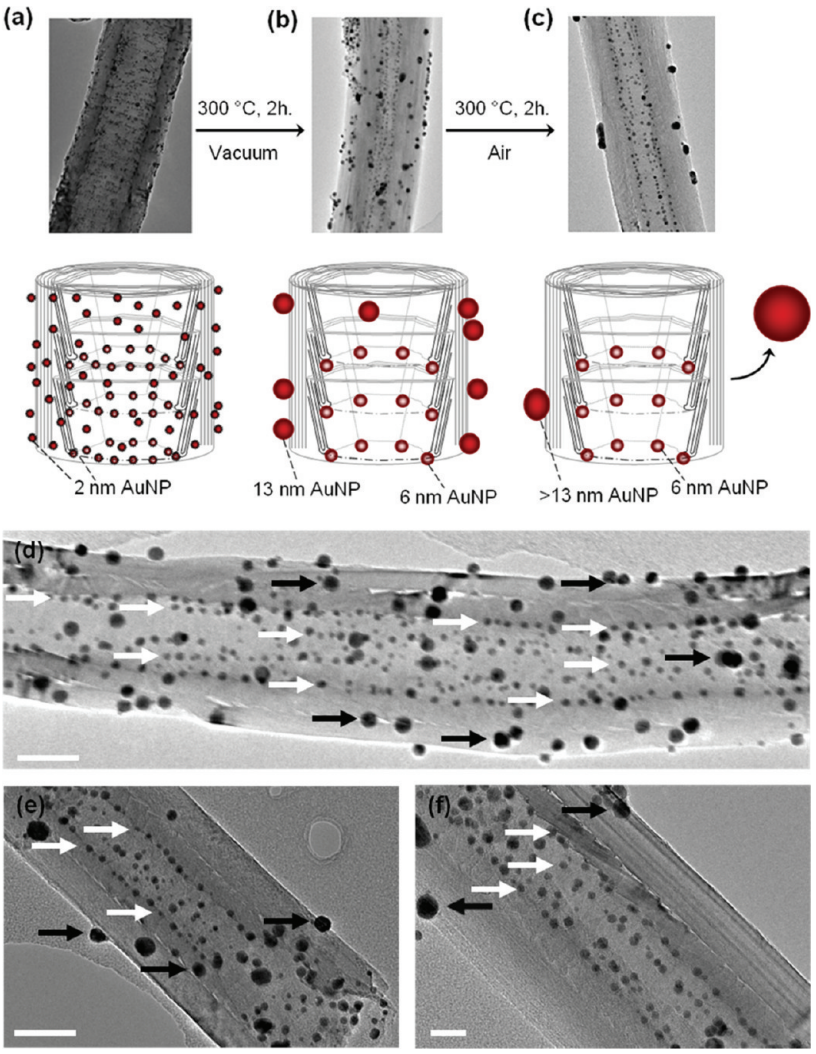

Figure 2. Bright-field TEM images and schematic diagrams illustrating the AuNPs adsorbed on the GNF outer surface (dark red) and anchored at the graphitic step-edges within the GNF (light red) taken; (a) immediately after the deposition of 2.3 nm AuNPs, (b) after heating the AuNP–GNF composite in vacuum at 300 °C for 2 h, and (c) after additional heating at 300 °C in air for a further 2 h, post-heating in vacuum. Bright-field TEM images of AuNPs grown from 2.3 nm AuNPs at 300 °C (d) on a heated stage TEM holder, or (e,f) in a furnace in vacuum. White and black arrows indicate AuNPs formed within the GNF cavity and on the GNF exterior surface, respectively. Scale bars are 50 nm in (d) and (e) and 20 nm in (f). TEM images were acquired using an accelerating voltage of 100 kV.

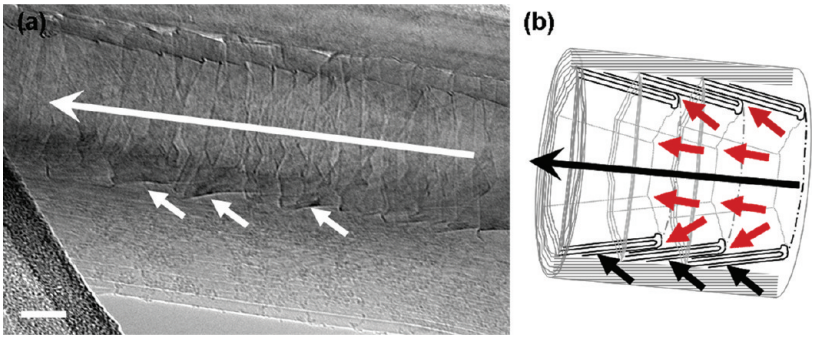

Figure 3. (a) Bright-field TEM image of a GNF showing the internal graphitic cone structure (short white arrows) which is formed by a few rolled-up layers of graphene. In contrast, the external surface, consisting of continuous cylindrical layers of graphene, is atomically smooth. (b) Schematic representation of a GNF. Short black arrows indicate the cone wall structure, the long arrow indicates the main axis of the GNF, and the red arrows show the possible anchoring points on the nanocone step-edges. Scale bar is 20 nm. TEM image was acquired using an accelerating voltage of 100 kV.

our imaging conditions, no observable changes in the specimen are induced by the e-beam, which ensures that the images represent the true structure of the specimen. However, when AuNP–GNF composites are

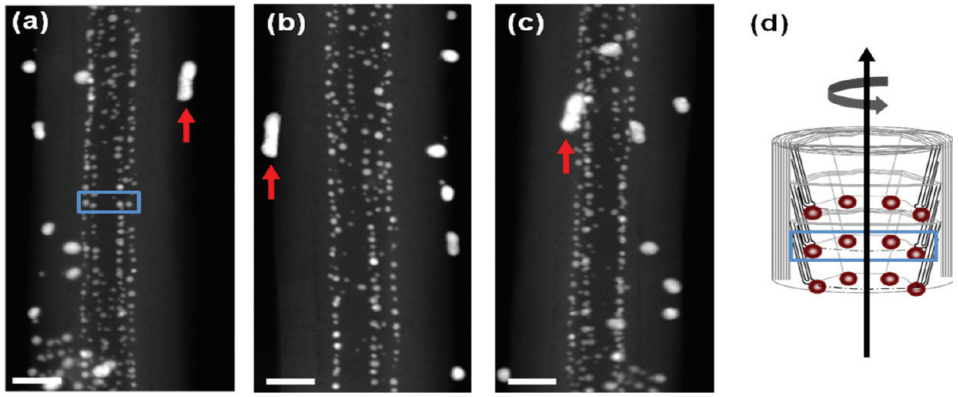

Figure 4. HAADF-STEM image tilt series showing thermally evolved AuNPs at tilt angles of (a) +60°, (b) 0°, and (c) −60° with respect to the host GNF. (d) Schematic representation of the AuNPs residing at the apexes of the facets. The blue rectangles in (a) and (d) highlight the AuNPs located at the apexes. During the tilt series, the 6 nm AuNPs remain located within the GNF cavity while AuNPs with diameters ≥13 nm change their positions with respect to the GNF interior. The red arrow indicates a small cluster of such AuNPs on the external surface. The scale bars are 50 nm. TEM image acquisition was performed using an accelerating voltage of 100 kV.

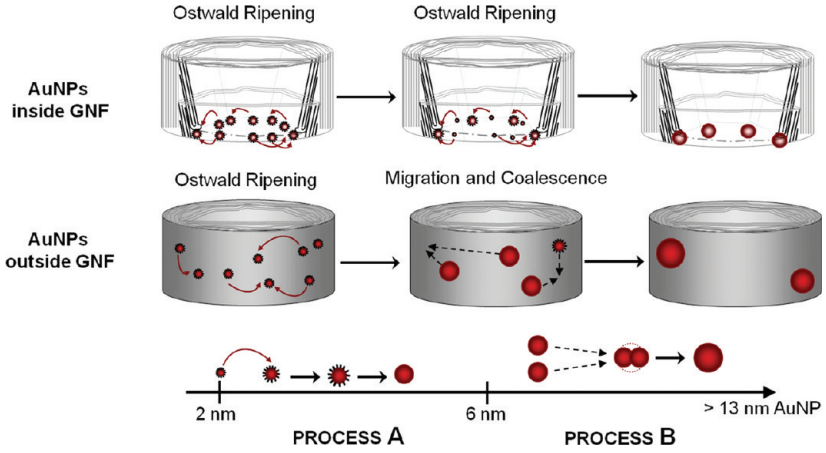

Figure 5. Schematic representations of the observed growth mechanisms of AuNPs in the internal cavity (above) and on the exterior surface (below) of GNFs. Ostwald ripening and nanoparticle migration events are indicated by solid and dashed arrows, respectively.

exposed to a high-energy e-beam (200 keV) with high flux (*ca.* 50 ρA/cm^2) for extended periods of time, the growth of nanoparticles can be triggered by the e-beam even at room temperature (Supporting Information, Figure S4). Interestingly, when AuNPs located inside GNFs are exposed to intensive e-beam irradiation, they grow to the same maximum size of *ca.* 6 nm as in the thermally activated experiments. The observation that, regardless of the source of energy providing the driving force for the AuNP transformation (heat or e-beam), AuNPs inside GNFs in vacuum always grow to the same maximum size indicates that the growth is controlled by the local structure of the graphene layers within the nanofiber.

In situ TEM imaging of the thermally activated transformation of AuNPs on the corrugated interior and the smooth exterior of GNFs in real time provides important information about the NP growth mechanisms. Our observations show that the processes of Ostwald ripening and nanoparticle coalescence coexist in AuNP−GNF structures. Ripening (mechanism A, Figure 5) is observed typically for smaller AuNPs (≤6 nm), where clusters of gold atoms diffuse from smaller AuNPs to larger AuNPs (Supporting Information). The migration and coalescence mechanism (B, Figure 5) appears to be dominant for AuNPs with sizes larger than 6 nm (Supporting Information). Since AuNPs adsorbed on the atomically smooth GNF exterior can migrate freely, they continue their growth beyond 6 nm. In contrast, migration of nanoparticles within GNF is inhibited due to the corrugated nature of the inner surface.

It is considered that the corrugated interior of the GNFs restricts the migration of nanoparticles within the cavity and thus precludes their growth *via* coalescence, so that Ostwald ripening remains the only possible growth mechanism for AuNPs inside the nanofiber. For the GNFs in this study, the typical height of the step-edges formed by the rolled-up graphene sheets is 3.3 ± 0.2 nm, and hence the surface area of contact between the AuNPs and GNF is maximized when the

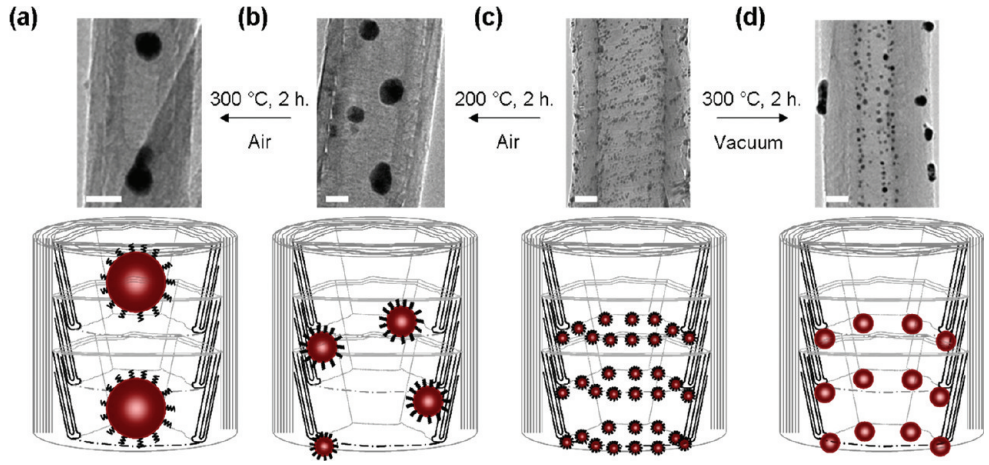

Figure 6. Bright-field TEM images and schematic diagrams of AuNPs in GNFs heated in air for 2 h at (a) 300 °C and (b) 200 °C, (c) alkylthiol-stabilized AuNP−GNF immediately after insertion of 2.3 nm AuNPs from $scCO_2$ and (d) uncoated AuNPs evolved in GNF by heating in vacuum at 300 °C for 2 h. Scale bars are 50 nm in (a) and 20 nm in (b−d). TEM images were acquired using an accelerating voltage of 100 kV.

AuNPs are located at the apexes of the graphitic facets of step-edges (Figures 3b and 4a,d), which leads to a drastic enhancement in the van der Waals interactions between the AuNPs and the carbon nanostructure.[33] This favorable interaction, occurring at the step-edges, immobilizes the nanoparticles, thus precluding their migration and thus growth above 6 nm in diameter.

The stability of the AuNPs thermally evolved on or in the GNFs in vacuum was examined in ambient environment by heating samples at 300 °C in atmospheric air (Figure 2c). Surface-adsorbed nanoparticles continued their growth beyond 13 nm when the AuNP−GNF composite was heated in air, often becoming elongated and detached from the GNF (Supporting Information, Figure S3), while AuNPs adsorbed inside the GNF retained their size and shape.

X-ray photoelectron spectroscopy (XPS) indicates complete removal of alkylthiol stabilizer from the AuNP surface after heating the AuNP−GNF composite in vacuum, so that direct contact between the metal surface of the nanoparticles and the GNF is established. This contact appears to be particularly effective at stabilizing the AuNPs adsorbed at step-edges. Normally, small metal nanoparticles (a few nanometers in diameter) are unstable at elevated temperature, but the 6 nm AuNPs adsorbed within the nanofiber exhibit remarkable stability up to 300 °C (Figures 2c, 4, and 6d).

Alkylthiol molecules, which have a high affinity for the surface of gold and hence are commonly employed as a protecting capping layer for AuNPs synthesized in solution, can influence the interactions between AuNPs and GNFs. When free-standing, alkylthiol-stabilized 2.3 nm AuNPs are inserted into GNFs from an $scCO_2$ solution, the stabilizer is also inserted into the nanofiber, as confirmed by XPS and thermal gravimetric analysis (TGA) measurements (Supporting Information, Figures S6−S10). During heating in vacuum, the surfactant molecules are fully and rapidly removed from the AuNP−GNF composite, but when AuNP−GNF is heated under atmospheric pressure, some of the alkylthiol remains inside the GNF. It is likely that the stabilizer impedes intimate contact between the metal surface of the AuNP and GNF that is required for stabilizing the nanoparticles at the step-edges. This leads to the continuous, unrestricted growth of the nanoparticles *via* migration and coalescence, until they reach the size of the internal cavity of the host GNF (Figure 6a,b).

Furthermore, in addition to structural factors, electronic factors may also play an important role in the stabilization of AuNPs. A recent study has demonstrated that the electrostatic interactions arising from charge transfer between the graphitic surface and gold nanoparticle can influence the size of the growing AuNPs.[34] It is interesting that the average size of nanoparticles was found to correlate with the number of graphene layers, with larger nanoparticles forming on thicker stacks of graphene.[34] Since in GNFs the tubular outer layer consists of a much thicker stack of graphene than the internal cones (Figure 3), our observation that smaller AuNPs are formed inside the nanofiber is consistent with the model developed for flat graphitic surfaces.[34]

In contrast to the random distribution of AuNPs on the GNF exterior surface, the nanoparticles inside the GNF form well-defined rows and columns. The rows are oriented perpendicular to the GNF cylinder axis and spaced by 6−9 nm from each other, which is commensurate with the lengths of the steps formed by the stacked cones. The columns of AuNPs, parallel to the GNF axis, reflect the faceted nature of the interior nanocone surface, as nanoparticles are preferentially positioned at the apexes of the facets (Figure 4a,d). In addition to the fact that the internal surface of the GNF has a significant stabilizing effect on the metal nanoparticles, which remain unchanged in air at 300 °C for over 2 h, the internal corrugations of the nanofiber

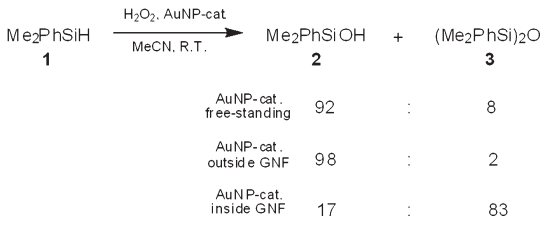

Scheme 1. AuNP-catalyzed silane oxidation by H_2O_2 and the effects of nanoparticle encapsulation in GNF on the distribution of products.

serve as effective templates for ordering AuNPs in two directions, parallel and perpendicular to the GNF axis.

Although the thermal treatment allows desorption from the GNF of the vast majority of the external AuNPs (Supporting Information, Figure S3), a small number of NPs still remain adhered to the nanofibers' outer surface. For specific practical applications of the NP−GNF composite, however, it is critical to ensure that all of the NPs are located inside. Hence, a selective procedure for the removal of the surface NPs, without affecting the encapsulated NPs, is highly desirable. We discovered that large nanoparticles could be effectively removed from the GNF surface by ultrasound. Thermally evolved AuNP−GNF composites subjected to an ultrasonic treatment in ethanol show selective desorption of AuNPs from the exterior surface (Supporting Information, Figure S11). Powder X-ray diffraction performed on bulk samples of ultrasound-cleaned AuNP−GNF indicates that only nanoparticles with a diameter of 6.2 nm (corresponding to the internal AuNPs) remain adsorbed (Supporting Information, Figure S11), which is consistent with TEM imaging (Figure 6d).

Nanoparticles inserted into GNF from supercritical fluid were shown to act as catalytic centers for the oxidation of silane by hydrogen peroxide (Scheme 1). The reaction of dimethylphenylsilane (**1**) leads to two products: dimethylphenylsilanol (**2**) and bis(dimethylphenyl)disiloxane (**3**). While the selectivity of gold nanoparticles adsorbed on the GNF outer surface is similar to that of free-standing AuNPs, favoring the formation of product **2**, the distribution of reaction products changes drastically for AuNPs encapsulated inside the nanofiber (Scheme 1). The enhanced production of **3** inside GNF can be explained by an increased local concentration of reactants within the GNF cavity, which is a general phenomenon observed in nanoreactors.[2] The formation of product **3** requires the collision of two dimethylphenylsilanol molecules, and therefore, any increase of concentration caused by the confinement in GNF will favor the formation of bis(dimethylphenyl)disiloxane. This control of chemical processes observed in GNFs illustrates the potential of carbon nanofibers as reaction nanovessels which are currently explored for preparative reactions by ourselves and others.[1,23]

CONCLUSION

Graphitized carbon nanofibers possessing different internal and external graphitic surfaces have been demonstrated as efficient host structures for nanoparticles of gold. Transformation of the deposited NPs can be activated directly on the GNFs using heat or an electron beam as the source of energy to promote the growth of the AuNPs. *In situ* TEM imaging allowed the two key mechanisms responsible for nanoparticle growth to be established: Ostwald ripening and migration followed by coalescence. The first process is prevalent for nanoparticles with diameters of 6 nm or less, whereas the second is significantly more important for larger NPs on the exterior surface. Graphitic step-edges forming the internal surface of GNF act to stabilize small NPs, restricting their migration and thus limiting their growth to 6 nm. Despite the fact that small metal nanoparticles are typically highly labile and metastable, AuNPs formed within GNFs exhibit no changes at temperatures as high as 300 °C. The presence of surfactant molecules (alkylthiols) within the GNF, however, can impede the interaction between AuNPs and the GNF, reducing the stabilizing effect of the graphitic step-edges and promoting further growth of the nanoparticles inside the GNF, being limited only by the space available within the nanofiber.

The ability to control the size and stability of nanoparticles by encapsulation in hollow nanofibers offers a new methodology for improving their thermal stability and for enhancing the functional performance of these otherwise metastable nanostructures. An additional benefit of the confinement within the GNF nanocontainers is the spontaneous ordering of NPs in two directions—across and along the GNF's channel. The ability to form rows and columns of well-organized equidistant and highly stable nanoparticles is highly desirable for catalytic, spintronic, data storage and photovoltaic applications.

EXPERIMENTAL SECTION

GNFs produced by chemical vapor deposition were purchased from Applied Science, USA. All other reagents and solvents were purchased from Sigma-Aldrich, UK, and used without further purification. Water was purified (>18.0 MΩ cm) using a Barnstead NANOpure II system. The experimental procedures followed for the preparation, insertion, and growth of the 2.3 nm AuNPs in vacuum, air, and *in situ* TEM are described in detail in the Supporting Information. The preparation of AuNPs required glassware to be cleaned with a mixture of concentrated hydrochloric and nitric acids (3:1 v/v, "aqua regia"), rinsed with deionized water, further cleaned with potassium hydroxide in methanol, and finally rinsed thoroughly with deionized water prior to use. HRTEM was performed using a JEOL 2100F transmission electron microscope (field emission

electron gun source, information limit 0.19 nm) using an accelerating voltage of 100 or 200 kV. TEM specimens were prepared by casting several drops of methanolic suspensions of the AuNP–GNF composite onto copper grid or nickel grid mounted "holey" carbon films and drying under a stream of nitrogen. The annular ring used for the *in situ* TEM experiment was a Gatan 652 double tilt-heating holder. Acquisition of TEM tilt series was performed using a Gatan 916 tomography holder and a Gatan double tilt beryllium holder. HAADF images were acquired using the JEOL digital STEM system. Statistical analysis was performed for each sample using Gatan Digital Micrograph software. By tilting the AuNP–GNF composites along the main nanofiber axis, in different regions of the specimen, the amount of encapsulated AuNPs was estimated for each area and averaged across the entire sample. Powder X-ray diffraction patterns were recorded using a Bruker D8 Advanced X-ray diffractometer equipped with Cu Kα source ($\lambda = 1.5418$ Å). Thermogravimetric analysis was determined using a TA Instrument equipped with a SDT Q600 analyzer under flowing air at a rate of 10 °C/min up to 800 °C. X-ray photoelectron spectra were recorded using a Kratos AXIS ULTRA with monochromated Al Kα radiation (10 kV anode potential, 15 A emission current) in fixed analyzer transmission mode (80 eV pass energy). Distribution of products in the reaction of AuNP-catalyzed oxidation of dimethylphenylsilane was determined by GC-MS, VG Autospec in EI^+ mode (Supporting Information, section S12).

Conflict of Interest: The authors declare no competing financial interest.

Acknowledgment. The authors thank the European Science Foundation, the European Research Council, the Royal Society, Marie Curie Fellowship scheme and the University of Nottingham for supporting this research, the Nottingham Nanoscience and Nanotechnology Centre for access to TEM facilities, and Dr. Nigel Neate and Keith Dinsdale for technical support. The authors acknowledge the use of the Kratos Axis ULTRA XPS in the School of Chemistry, and Emily Smith for running the samples and helpful discussions on data interpretation.

Supporting Information Available: Synthesis and characterization of alkanethiolate-stabilized AuNPs, procedure for insertion of AuNPs into GNFs using supercritical CO_2, description of the vacuum system used for thermal evolution of AuNPs on GNFs, procedure for sealing of AuNP–GNF in vacuum, procedure for heating of the samples on a TEM grid under vacuum, procedure for heating of the bulk AuNP–GNF material under vacuum, procedure of thermal desorption of AuNPs from GNFs, observation of ripening of AuNPs in GNFs activated by electron beam irradiation, *in situ* TEM measurements in real time, X-ray photoelectron spectroscopy measurements and thermal gravimetric analysis for AuNP–GNF composites, procedure for selective removal of AuNPs from GNF surface and powder X-ray diffraction measurements for the resultant AuNP–GNF composite, oxidation of silanes catalyzed by gold nanoparticles. This material is available free of charge *via* the Internet at http://pubs.acs.org.

REFERENCES AND NOTES

1. Serp, P.; Castillejos, E. Catalysis in Carbon Nanotubes. *ChemCatChem* **2010**, *2*, 41–47.
2. Pan, X.; Bao, X. The Effects of Confinement Inside Carbon Nanotubes on Catalysis. *Acc. Chem. Res.* **2011**, *44*, 553–562.
3. Datta, S.; Marty, L.; Cleuziou, J. P.; Tilmaciu, C.; Soula, B.; Flahaut, E.; Wernsdorfer, W. Magneto-Coulomb Effect in Carbon Nanotubes Quantum Dots Filled with Magnetic Nanoparticles. *Phys. Rev. Lett.* **2011**, *107*, 186804.
4. Li, B. D.; Wang, C.; Yi, G. Q.; Lin, H. Q.; Yuan, Y. Z. Enhanced Performance of Ru Nanoparticles Confined in Carbon Nanotubes for CO Preferential Oxidation in a H_2-Rich Stream. *Catal. Today* **2011**, *164*, 74–79.
5. Cleuziou, J. P.; Wernsdorfer, W.; Ondarcuhu, T.; Monthioux, M. Electrical Detection of Individual Magnetic Nanoparticles Encapsulated in Carbon Nanotubes. *ACS Nano* **2011**, *5*, 2348–2355.
6. Kang, J. W.; Kim, K. S.; Kwon, O. K.; Hwang, H. J. Linear Nanomotor Based on Electromigration of a Nanoparticle Encapsulated in a Carbon Nanotube. *Nanosci. Nanotechnol.* **2011**, *11*, 1573–1576.
7. Wang, J.; Beeli, P.; Ren, Y.; Zhao, G. M. Giant Magnetic Moment Enhancement of Nickel Nanoparticles Eembedded in Multiwalled Carbon Nanotubes. *Phys. Rev. B* **2010**, *82*, 193410.
8. Roa, D. B.; Barcelos, I. D.; de Siervo, A.; Pirota, K. R.; Lacerda, R. G.; Magalhaes-Paniago, R. Observation of Ferromagnetism in PdCo Alloy Nanoparticles Encapsulated in Carbon Nanotubes. *Appl. Phys. Lett.* **2010**, *96*, 253114.
9. Guo, S. J.; Pan, X. L.; Gao, H. L.; Yang, Z. Q.; Zhao, J. J.; Bao, X. H. Probing the Electronic Effect of Carbon Nanotubes in Catalysis: NH_3 Synthesis with Ru Nanoparticles. *Chem.—Eur. J.* **2010**, *16*, 5379–5384.
10. Gan, L.; Lv, R.; Du, H. D.; Li, B. H.; Kang, F. Y. Highly Dispersed Pt Nanoparticles by Pentagon Defects Introduced in Bamboo-Shaped Carbon Nanotube Support and Their Enhanced Catalytic Activity on Methanol Oxidation. *Carbon* **2009**, *47*, 1833–1840.
11. Qin, Y.; Liu, L. F.; Yang, R. B.; Gosele, U.; Knez, M. General Assembly Method for Linear Metal Nanoparticle Chains Embedded in Nanotubes. *Nano Lett.* **2008**, *8*, 3221–3225.
12. Monch, I.; Leonhardt, A.; Meye, A.; Hampel, S.; Kozhuharova-Koseva, R.; Elefant, D.; Wirth, M. P.; Buchner, B. Synthesis and Characteristics of Fe-Filled Multi-Walled Nanotubes for Biomedical Application. *Proc. Int. Conf. Nanosci. Tech.* **2007**, *61*, 820–824.
13. Banhart, F.; Grobert, N.; Terrones, M.; Charlier, J. C.; Ajayan, P. M. Metal Atoms in Carbon Nanotubes and Related Nanoparticles. *Int. J. Modern Phys. B* **2001**, *15*, 4037–4069.
14. Ratanatawanate, C.; Xiong, C.; Balkus, K., Jr. Fabrication of PbS Quantum Dot Doped TiO_2 Nanotubes. *ACS Nano* **2008**, *2*, 1682–1688.
15. Ratanatawanate, C.; Tao, Y.; Balkus, K., Jr. Photocatalytic Activity of PbS Quantum Dot/TiO_2 Nanotube Composites. *J. Phys. Chem. C* **2009**, *113*, 10755–10760.
16. Tsang, S. C.; Chen, Y. K.; Harris, P. J. F.; Green, M. L. H. A Simple Chemical Method of Opening and Filling Carbon Nanotubes. *Nature* **1994**, *372*, 159–162.
17. Ajayan, P. M.; Iijima, S. Capillarity-Induced Filling of Carbon Nanotubes. *Nature* **1993**, *361*, 333–334.
18. Ajayan, P. M.; Colliex, C.; Lambert, J. M.; Bernier, P.; Barbedette, L.; Tence, M.; Stephan, O. Growth of Manganese Filled Carbon Nanofibres in the Vapour-Phase. *Phys. Rev. Lett.* **1994**, *72*, 1722–1725.
19. Ugarte, D.; Chatelain, A.; de Heer, W. A. Nanocapillarity and Chemistry in Carbon Nanotubes. *Science* **1996**, *274*, 1897–1899.
20. Huang, H.; Kajiura, H.; Murakami, Y.; Ata, M. Metal Sulphide Catalyzed Growth of Carbon Nanofibres and Nanotubes. *Carbon* **2003**, *41*, 615–618.
21. Costa, P. M. F. J.; Sloan, J.; Rutherford, T.; Green, M. L. H. Encapsulation of Re_xO_y Clusters within Single-Walled Carbon Nanotubes and Their in Tubulo Reduction and Sintering to Re Metal. *Chem. Mater.* **2005**, *17*, 6579–6582.
22. Wang, C.; Guo, S.; Pan, X.; Chen, W.; Bao, X. Tailored Cutting of Carbon Nanotubes and Controlled Dispersion of Metal Nanoparticles Inside Their Channels. *J. Mater. Chem.* **2008**, *18*, 5782–5786.
23. Castillejos, E.; Debouttiere, P.-J.; Roiban, L.; Solhy, A.; Martinez, V.; Kihn, Y.; Ersen, O.; Philippot, K.; Chaudret, B.; Serp, P. An Efficient Strategy To Drive Nanoparticles into Carbon Nanotubes and the Remarkable Effect of Confinement on Their Catalytic Performance. *Angew. Chem., Int. Ed.* **2009**, *48*, 2529–2533.
24. La Torre, A.; Rance, G. A.; El Harfi, J.; Li, J.; Irvine, D. J.; Brown, P. D.; Khlobystov, A. N. Transport and Encapsulation of Gold Nanoparticles in Carbon Nanotubes. *Nanoscale* **2010**, *2*, 1006–1010.
25. Castillejos, E.; Chico, R.; Bacsa, R.; Coco, S.; Espinet, P.; Perez-Cadenas, M.; Guerrero-Ruiz, A.; Rodriguez-Ramos, I.; Serp, P. Selective Deposition of Gold Nanoparticles on or Inside Carbon Nanotubes and Their Catalytic Activity for

Preferential Oxidation of CO. *Eur. J. Inorg. Chem.* **2010**, 5096–5102.
26. Rosenfeld, G.; Morgenstern, K.; Beckmann, I.; Wulfhekel, W.; Laegsgaard, E.; Besenbacher, F.; Comsa, G. Stability of Two-Dimensional Clusters on Crystal Surfaces: From Ostwald Ripening to Single-Cluster Decay. *Surf. Sci.* **1998**, *402*, 401–408.
27. Morgenstern, K.; Rosenfeld, G.; Laegsgaard, E.; Besenbacher, F.; Comsa, G. Measurement of Energies Controlling Ripening and Annealing on Metal Surfaces. *Phys. Rev. Lett.* **1998**, *80*, 556–559.
28. Meyer, R.; Ge, Q.; Lockemeyer, J.; Yeates, R.; Lemanski, M.; Reinalda, D.; Neurock, M. An *Ab Initio* Analysis of Adsorption and Diffusion of Silver Atoms on Alumina Surfaces. *Surf. Sci.* **2007**, *601*, 134–145.
29. Heilmann, A.; Werner, J. *In Situ* Observation of Microstructural Changes of Embedded Silver Particles. *Thin Solid Films* **1998**, *317*, 21–26.
30. Wynblatt, P.; Gjostein, N. A. Particle Growth in Model Supported Metal-Catalysts 0.1. Theory. *Acta Metall.* **1976**, *24*, 1165–1174.
31. Zhu, L.; Lu, G.; Mao, S.; Chen, J.; Dikin, D. A.; Chen, X.; Ruoff, R. S. Ripening of Silver Nanoparticles on Carbon Nanotubes. *NANO* **2007**, *2*, 149–156.
32. Brust, M.; Walker, M.; Bethell, D.; Schiffrin, D. J.; Whyman, R. Synthesis of Thiol-Derivatized Gold Nanoparticles in a 2-Phase Liquid–Liquid System. *J. Chem. Soc., Chem. Commun.* **1994**, 801–802.
33. Rance, G. A.; Marsh, D. H.; Bourne, S. J.; Reade, T. J.; Khlobystov, A. N. van der Waals Interactions between Nanotubes and Nanoparticles for Controlled Assembly of Composite Nanostructures. *ACS Nano* **2010**, *4*, 4920–4928.
34. Luo, Z.; Somers, L. A.; Dan, Y.; Ly, T.; Kybert, N. J.; Mele, E. J.; Johnson, A. T. C. Size-Selective Nanoparticle Growth on Few-Layer Graphene Films. *Nano Lett.* **2010**, *10*, 777–781.